ORIGINAL PAPER

CrossMark

Effect of N and Zr on as-cast microstructure and properties after annealing of a high-speed steel

Hao-ran Cui[1] · Jian-ping Lai[1] · Qing-lin Pan[1] · Xiang-dong Wang[1]

Abstract

Effects of N and Zr on the as-cast microstructure and properties after annealing of high-speed steel (HSS) were investigated by using electronic probe micro-analysis, Rockwell hardness test, X-ray diffractometry and differential scanning calorimetry with combination of microstructure analysis. The results indicate that the addition of N and Zr will refine the eutectic structures and enhance the stability of carbides which are mainly MC, M_2C and M_7C_3. The coarse dendritic structures decrease significantly and most of the carbides are distributed in the microstructure uniformly. Moreover, a kind of Zr–Si compound which only exists in VC is discovered, and this new phase is speculated to be related with the spheroidization of VC. The annealing process is set up to 6 different time periods which are 1, 3, 6, 10, 15 and 20 h, respectively. In different annealing processes at 750 °C which is lower than austenitizing temperature, the addition of N and Zr makes the decrease of hardness more obvious and restrains the precipitation of secondary carbides with the extension of time. Moreover, when the annealing time reaches 20 h, some clusters appear in the matrix of the two samples, and the density of clusters in HSS1 is lower, but the matrix of HSS1 contains more C and alloying elements which indicate more carbides precipitate.

Keywords N addition · Zr addition · High-speed steel · As-cast microstructure · Precipitation · Annealing

1 Introduction

High-speed steel (HSS) has become popular and has been extensively used domestically and overseas in recent years [1, 2]. Compared with traditional steels, high-speed steel possesses excellent combination of hardness, wear resistance, and high-temperature properties, which are related to various complex eutectic carbides [3, 4]. Factors such as chemical composition and cooling rate have a certain impact on the morphology and distribution of carbides, while the characteristics of carbide also have effect on the mechanical properties of high-speed steel [5–7]. Micro-alloying is an effective way to improve the microstructure and properties of the alloys by optimizing the carbides. Previous studies include various carbides-forming elements, such as Nb [8, 9] and Ti [10, 11]. The addition of

niobium or titanium to high-speed steel gives priority to the formation of NbC and TiC, of which the hardness is higher than that of other carbides. The formation of NbC or TiC also reduces the carbon content of the matrix, thus improving toughness and wear resistance. As the alloying elements, N and Zr are added into the high-speed steel to modify the morphology, composition and volume fraction of carbides in order to optimize the performance of the steel [12–15]. So far, the exploration of HSS with N and Zr micro-alloying has a certain foundation, but there are few investigations on how the addition of N and Zr influences the microstructure transformations and morphologies of carbides in high-speed steel. As a result, it is necessary to explore the influence of N and Zr on the as-cast microstructure.

The HSS cast is likely to show segregation and nonuniformity in microstructure which is lack of refining grains on account of the direct molding. On the other hand, the workpiece of centrifugal casting high-speed steel roll is likely to produce large stresses due to the compound casting process. In addition, the hardness of as-cast HSS is

✉ Qing-lin Pan
  pql102@126.com

1   School of Materials Science and Engineering, Central South University, Changsha 410083, Hunan, China

too high to meet the requirements of subsequent rough machining processes, so the centrifugal casting HSS is necessary to eliminate these defects by annealing process. However, the researches on the heat treatment of high-speed steel are mostly concentrated on the quenching and tempering processes. In this paper, the effect of N and Zr on the as-cast microstructure is investigated in details. Moreover, the effect of N and Zr on the properties after different annealing processes is also studied.

2 Experimental

The compositions of two sets of HSS samples for experiments are listed in Table 1. The first sample without N and Zr is named HSS0, and the second sample which contains N and Zr is named HSS1. They are melted in a vacuum induction furnace with an argon balance and deoxidized by Al and Si–Ca alloys. Afterward, N and Zr alloys are added to the molten HSS1 until the demand for component content is met. Then, the molten steel is poured into horizontal centrifugal casting machine with dimension of $\phi200$ mm $\times$ 300 mm for centrifugal casting. The cast will be taken out when the temperature of the cast is below 100 °C and then cooled in still air. The process of retrieving samples is shown in Fig. 1. The metallographic specimens (10 mm $\times$ 10 mm $\times$ 10 mm) are cut out from the cast. All the experimental analyses are carried out on A side. Microstructure is observed by scanning electron microscopy (SEM), and the analyses of elements in the matrix and carbides are examined by the electronic probe micro-analyzer (EPMA). X-ray diffraction (XRD) is used for the analysis of different phases and carbides.

The phase transformation temperatures are measured using differential scanning calorimetry (DSC) with a heating rate of 10 °C/min to establish a suitable annealing temperature (750 °C). On the other hand, two samples are cut into cubes with the size of 30 mm $\times$ 30 mm $\times$ 30 mm for annealing. The samples are annealed at 750 °C for 1, 3, 6, 10, 15 and 20 h, respectively, and then cooled in the air. The hardness of the samples after annealing process is measured by Rockwell hardness tester. The variations of microstructure and element contents in matrix which are caused by different lengths of annealing time are observed by SEM and EPMA.
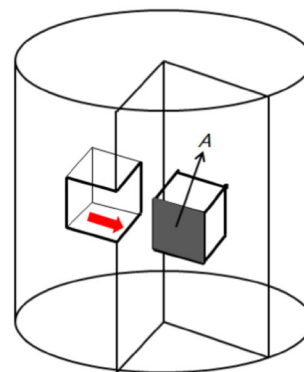

Fig. 1 A schematic drawing of retrieving samples from cast

3 Results and discussion

3.1 As-cast microstructure

The microstructures of the two samples are shown in Fig. 2. By comparison, in the microstructure of HSS0, it can be observed that some dendrites are surrounded by semi-continuous interdendritic networks of eutectic carbides. Some large pieces of carbide and the chrysanthemum-like eutectic communities can also be observed. However, the large-size carbides which have nonuniform distribution are bad for the toughness property of HSS [16]. In the microstructure of HSS1, the large pieces of carbide are significantly reduced and chrysanthemum-like eutectic communities disappear basically. Moreover, the dendrites become smaller and isolated. The short rods and striped carbides in HSS0 evolve into spherical and small pieces of carbides with a mean diameter of 5–6 μm and smooth interfaces which exhibit higher stability [17]. The laminas of the curve lamellar carbides become parallel to each other after the addition of N and Zr. As a result, the whole structures become more uniform. Both of the two samples are distributed of some needle-like martensite in the matrix. According to the above results, it can be concluded that the as-cast microstructure of HSS shows a significant refinement after the addition of N and Zr.

Figure 3 shows the X-ray spectra of HSS0 and HSS1. It is found that the two samples are similar in phase compositions. However, some diffraction peaks of carbides and retained austenite become weaker in HSS1, which may be related to the decrease of the large pieces of carbides.

Table 1 Chemical compositions of two samples (wt%)

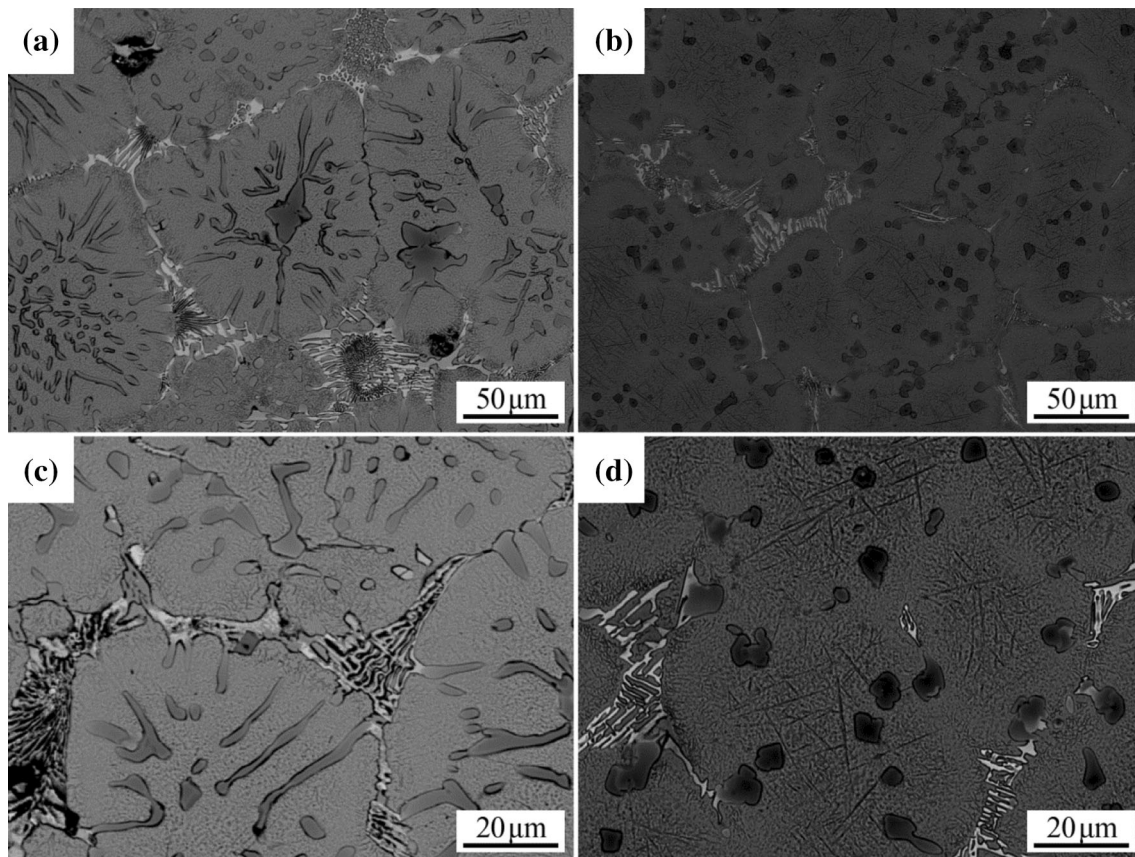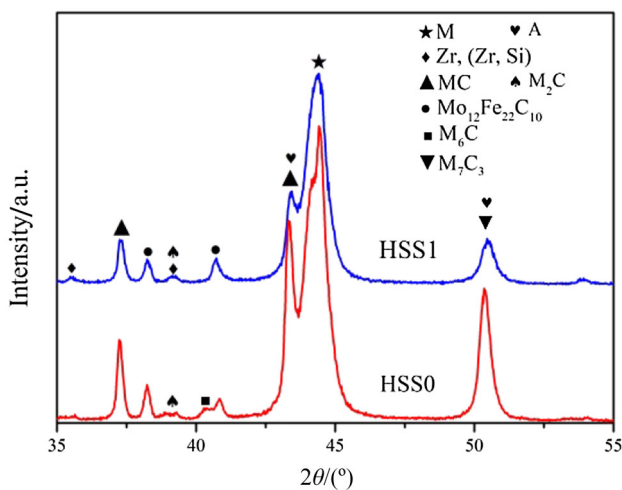| Alloy	C	V	Mo	Cr	W	Si	N	Zr	Fe
HSS0	1.85	5.87	3.81	4.78	1.41	1.38	–	–	Balance
HSS1	1.82	5.86	3.85	4.83	1.35	1.42	0.38	1.23	Balance

Fig. 2 As-cast microstructures of HSS0 (a, c) and HSS1 (b, d)

Fig. 3 XRD spectra of HSS0 and HSS1

$Mo_{12}Fe_{22}C_{10}$ which belongs to a kind of eutectic cementite exists in both samples and its diffraction peaks remain essentially unchanged. Furthermore, it can be observed that Zr and a new phase (Zr, Si) which may be a kind of compound of Zr and Si appear in HSS1. In this context, a detailed analysis will be given below. According to the result of XRD, the matrix of the microstructure should be

martensite (M) which is in agreement with Fig. 2, and the types of carbides are all presented. To further clarify composition of the large pieces of carbides in HSS0 according to the previous results, the high precision elemental quantitative analysis of the carbides was detected by EPMA. As shown in Fig. 4 and Table 2, it can be observed that a large piece of carbide with irregular shapes exists in HSS0. The distribution of elements in the carbide is uneven; thus, it can be calculated that this large piece of carbide may be formed by several kinds of eutectic carbides. Referring to Table 2, some fishbone-shaped carbides with a ridge-line exist in Point 1. This is the representative morphology of M_6C, and the content of W in Point 1 is higher than that of others. It is speculated that the carbides here may be $(W, Fe)_6C(M_6C)$. On the other side, the content of Mo in Point 2 is high, while the content of V is low. Moreover, it can be observed that some curve lamellar carbides are around Point 2. M_2C carbides could form this structure under certain conditions [7]. Thus, the carbides here may be $Mo_2C(M_2C)$. According to the above results, this large piece of carbide is supposed to be composed of $(W, Fe)_6C(M_6C)$ and $Mo_2C(M_2C)$. As shown in Fig. 4b and Table 2, the content of V and C is very high in Point 4, so the carbides here could be VC. Their shapes are

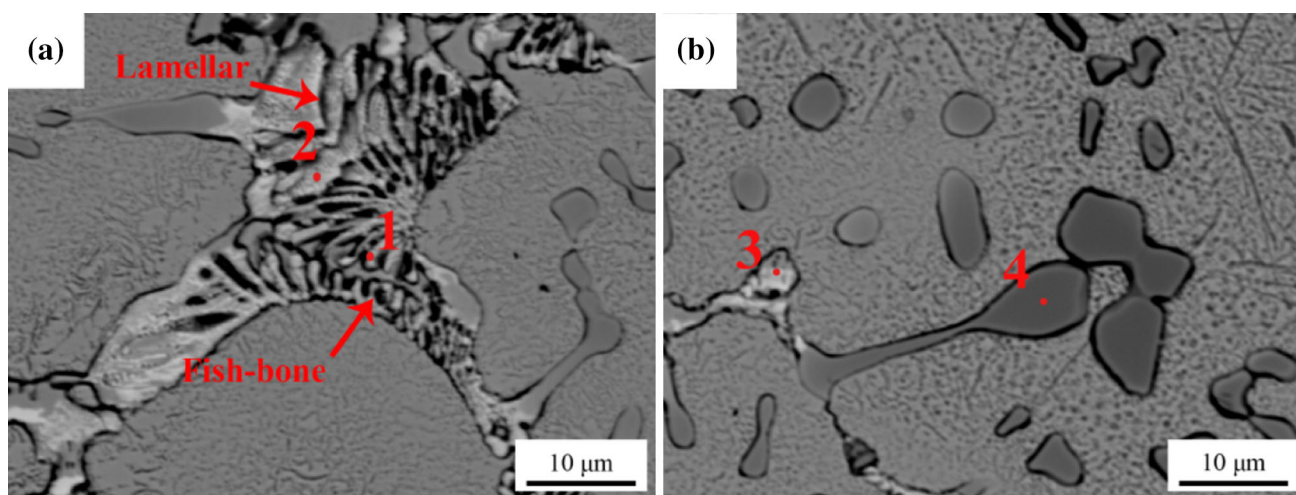**Fig. 4** Microstructure of carbides in HSS0

Table 2 Elemental analysis of carbides in Fig. 3 (at.%)

Point No.	C	Cr	V	Mo	W
1	12.0	14.1	5.8	12.3	14.4
2	6.9	18.8	9.1	34.7	9.5
3	23.5	23.5	11.5	21.2	2.5
4	40.6	3.0	51.8	2.6	0.8

irregular and some of them are not completely isolated from each other. The content of Cr in Point 3 is the highest; thus, the carbides on the "petal" of the chrysanthemum-like communities may be $(Cr, Fe)_7C_3(M_7C_3)$.

Figure 5 shows the mapping scanning distribution of N, Zr and some other elements in HSS1 analyzed by EPMA. It is observed that N is distributed in microstructure homogeneously but more abundant in spherical VC particles in Fig. 5a. However, Zr is only concentrated in the VC but not dissolved in the matrix. Most of Si is evenly distributed in the matrix, but it is noteworthy that the distribution of Si coincides well with the distribution of Zr in certain VC particles. In Fig. 5b, a composition coincident point of Si and Zr is shown more clearly. It can be inferred that the coincident point should be a kind of compound. From the results of Fig. 6, it can be seen that there are two significant and coincident peaks of Zr and Si in the area where the color is dark in the VC particles, so the presence of this compound is more certain. In Table 3, it can be seen that the contents of Si and Zr are higher in the dark area while there are no Si and Zr in the light area substantially. Therefore, it can be speculated that this small dark particle with diameter of about 2 µm inside the VC is Zr–Si compound.

In conclusion, the distribution of N and Zr is concentrate in VC; moreover, the Zr–Si compound generates and only

exists in VC, so it can be speculated that the existence of the compound may play an important role in the spheroidization of VC in HSS1. Regarding this phase, after all, further research is necessary.

DSC curves of two samples in the process of heating schedule are shown in Fig. 7a, and a distinct endothermic peak can be observed in the temperature at around 850 °C in both curves. The peak should correspond to $\alpha \rightarrow \gamma$ transformation [18]. It can be found that the onset of $\alpha \rightarrow \gamma$ which is designated as the A_{c1} temperature is about 825 °C and the transformation off-set denoted as A_{c3} temperature is about 875 °C. In addition, the peak at about 760 °C is not obvious. It may be attributed to ferromagnetic $\rightarrow$ paramagnetic transformation of the α-ferrite upon reaching T_C, the Curie temperature. It may also be caused by some carbides precipitated from carbon-saturated martensite [19–21]. For this peak, more in-depth research is needed to fully explain it.

Figure 7b shows the higher temperature range of two samples, about 1000–1250 °C. HSS0 shows three obvious endothermic peaks, which show the dissolution of carbides. There are three kinds of carbides (MC, M_7C_3 and M_2C) in the initial microstructure, so the three peaks should be relevant to these carbides, respectively [3, 4]. Because M_2C eutectic carbide is a metastable phase which is much less stable than M_7C_3 and MC carbides, it tends to decompose at high temperatures, and the MC carbides are the most stable. By contrast, there are two faint and partially overlapped endothermic peaks in the DSC curve of HSS1. That is because the solubility product of vanadium nitride is lower than that of vanadium carbide. It prefers to form vanadium nitride in HSS, which adds N and stabilizes the energy in consideration of thermodynamics; thus, the carbides in HSS1 exhibit higher stability [22, 23]. In the previous comparison of the metallographic photographs of
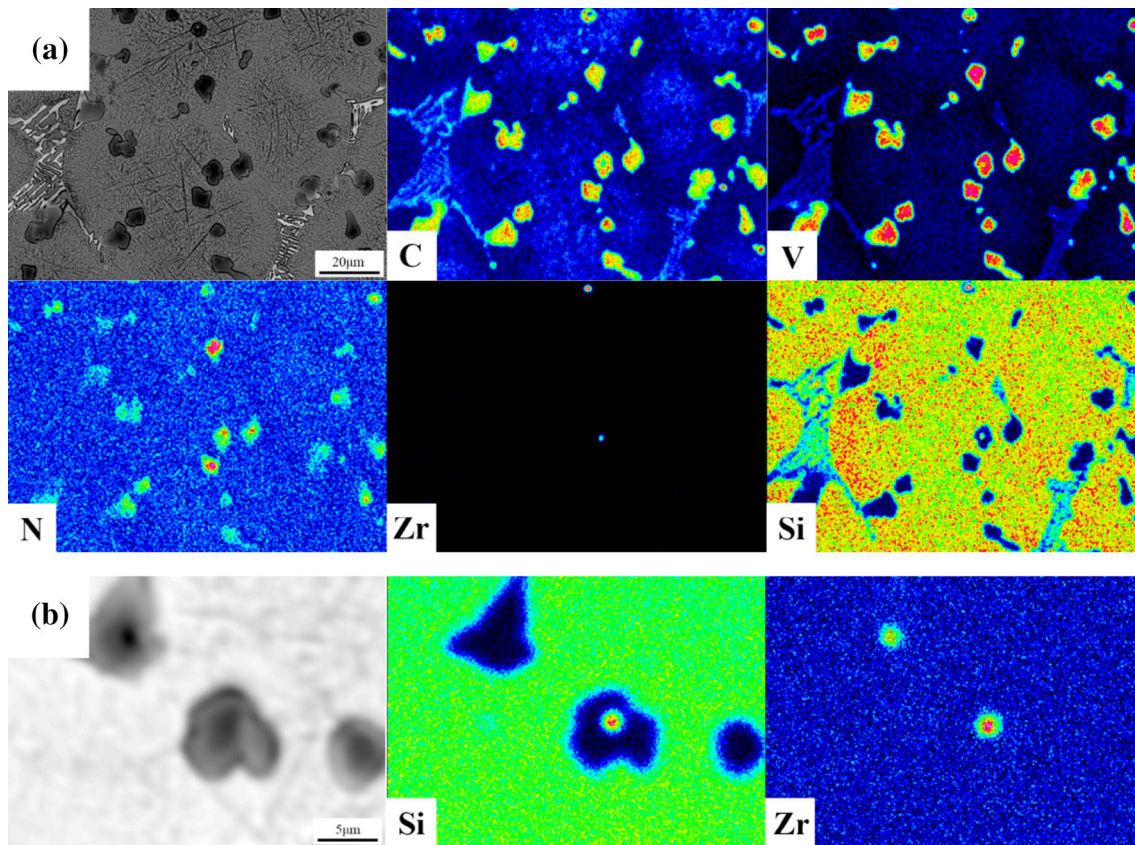
Fig. 5 Distribution of elements in microstructure of HSS1 analyzed by EPMA
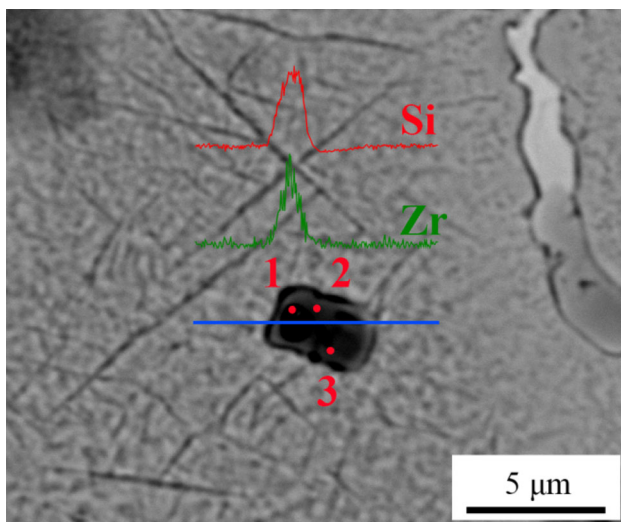

Fig. 6 Line scanning of a VC particle which contains Zr–Si compound by EPMA

HSS0 and HSS1, it can also be found that the carbides in HSS1 which have morphologies of smooth interfaces exhibit a higher stability. As a result, the existence of carbides dissolution taking place for higher temperatures makes the peaks to be partially overlapped.

Table 3 Elemental analysis of VC particle in Fig. 5 (wt%)

| Point No.	Si	Zr	C	V
1	2.6	2.7	12.4	70.1
2	1.2	2.1	10.7	70.0
3	0.1	0.1	13	74.5

3.2 Annealing process

The purpose of annealing for HSS is to make the chemical composition and structure of the steel more uniform and closer to the equilibrium state, and to reduce the hardness and improve the cutting performance. Thus, the annealing process does not require phase transitions, and the annealing temperature can be set up at the temperature lower than A_{c1}. According to the DSC curves, the annealing temperature is set up at 750 °C in this experiment. Two samples are subjected to 6 time periods for annealing and then measured hardness. The curves which described the change in hardness due to the different annealing time are drawn in Fig. 8.

It can be seen from Fig. 8 that the as-cast hardness of HSS0 and HSS1 is 64 HRC and 64.5 HRC, respectively.
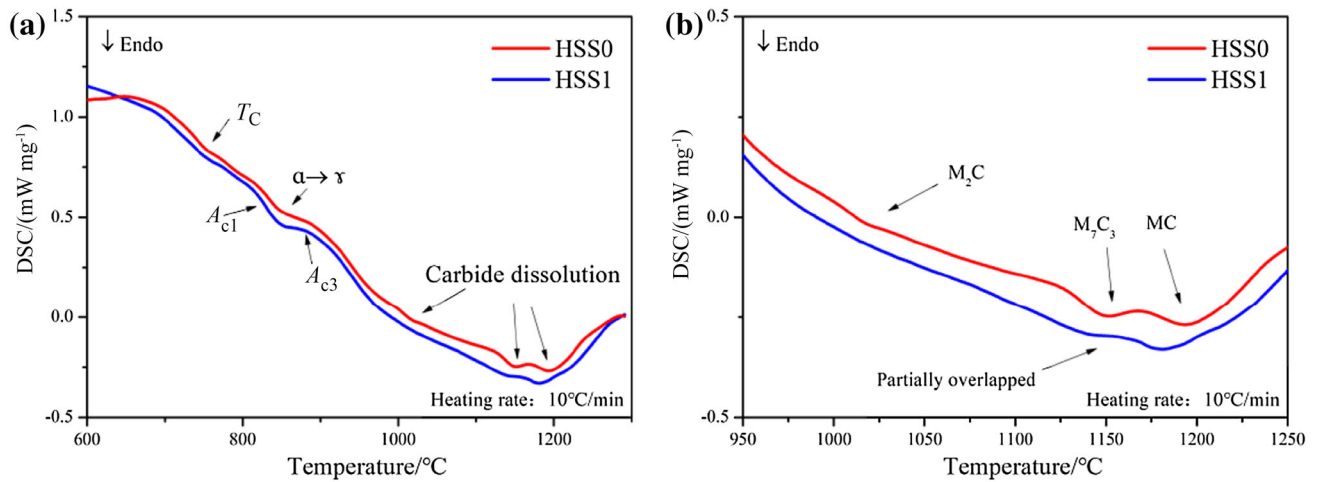
Fig. 7 DSC curves of as-cast HSS0 and HSS1 (**a**) and expanded portrayal of DSC curves around 1100 °C (**b**)
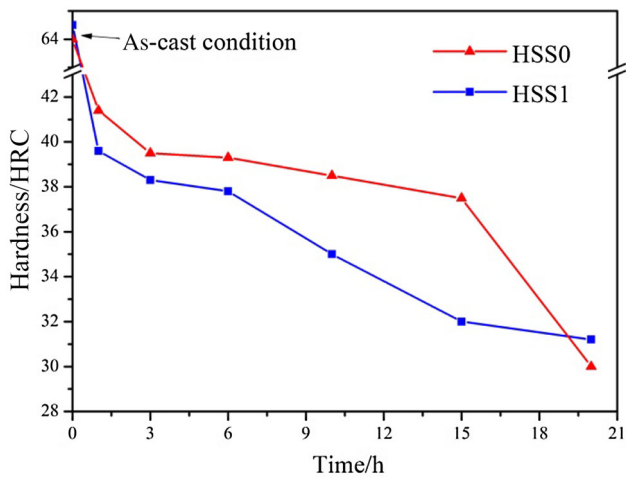

**Fig. 8** Change of hardness of HSS0 and HSS1 due to different annealing time

Both samples have high hardness values. Because the centrifugal casting of high-speed steel was cast in the mold with a fast cooling speed, the as-cast structure is similar to the quenched structure which is composed of non-equilibrium phases including primary carbides, martensite and retained austenite. The presence of martensite makes the as-cast HSS possess high hardness. When annealed for 1 h, the hardness of the two samples decreases sharply. With the extension of annealing time, the hardness of HSS1 decreases obviously; however, the hardness of HSS0 decreases slightly as before. The hardness of HSS0 begins to decrease significantly only when the annealing time reaches 20 h, while for the HSS1, the hardness decreases slightly.

The microstructural evolution of HSS during annealing process is similar to that of tempering process, when the primary carbides do not change, and the martensite and retained austenite are dissolved [24]. Therefore, the matrix of the two samples after different annealing processes was analyzed by SEM, and the element analysis was made in the matrix area with a diameter of 20 μm. As shown in Fig. 9a, b, the needle-like martensite in the two samples is both greatly reduced and transforms into ferrite after annealing for 1 h. There are some weeny secondary carbides which are usually MC and/or M_2C that can be observed in the matrix as well [25]. The matrix which is composed of ferrite and cementite that mix with carbides particles may be sorbite. During the annealing process, retained austenite decomposes into ferrite and secondary carbides; meanwhile, the carbon and alloying elements which were originally dissolved in the martensite matrix are precipitated and result in the decline in saturation of martensite; thus, the hardness of α-phase decreases, and macrohardness decreases subsequently. In Fig. 9c, d, the needle-like α-phase disappears completely and more weeny carbides are precipitated and grow up in two samples. Moreover, it can also be seen in Fig. 10 that the content of C in the matrix of two samples increases due to the precipitation of carbides when the annealing time extends to 6 h. In general, there is no big difference between two samples when the annealing time is less than 6 h, but then the content of C in HSS0 increases continuously with the extension of annealing time, while the content of C presents a steady state in HSS1. From Fig. 9e, it can be seen that the some secondary carbides precipitate and grow up in HSS0, which is probably because the extension of annealing time aggravates the desolation of carbons as well as alloying elements and more carbides precipitate. The precipitation of secondary carbides causes the hardness of HSS0 to decrease slightly and the C content to increase in this period. On the contrary, no obvious large carbides precipitate in Fig. 9f and the matrix is sparsely
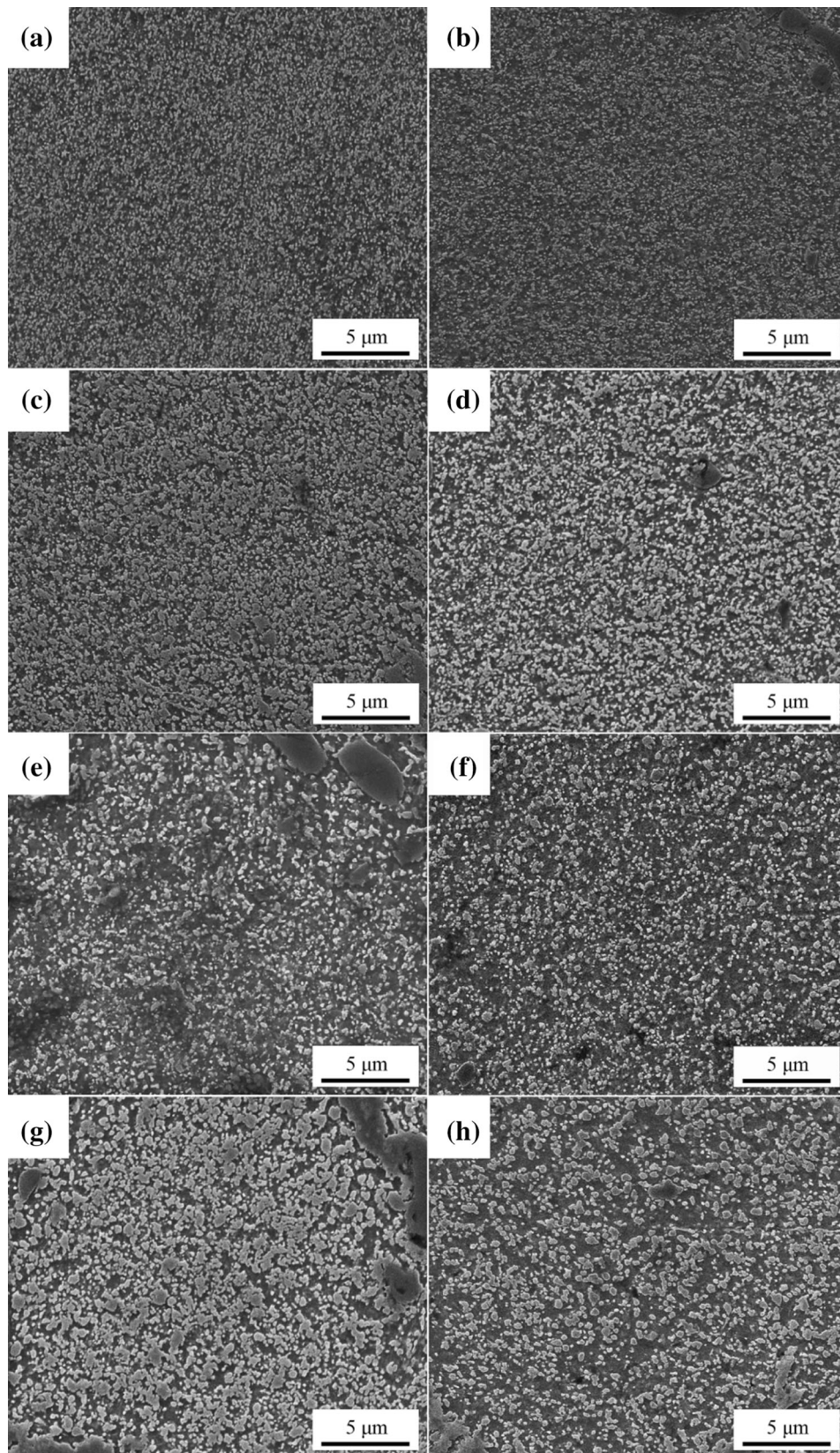
Fig. 9 Matrix microstructure of HSS0 and HSS1 with different annealing time at 750 °C. **a**, **c**, **e**, **g** Matrix of HSS0 after annealing for 1, 6, 15, and 20 h, respectively; **b**, **d**, **f**, **h** matrix of HSS1 after annealing for 1, 6, 15, and 20 h, respectively
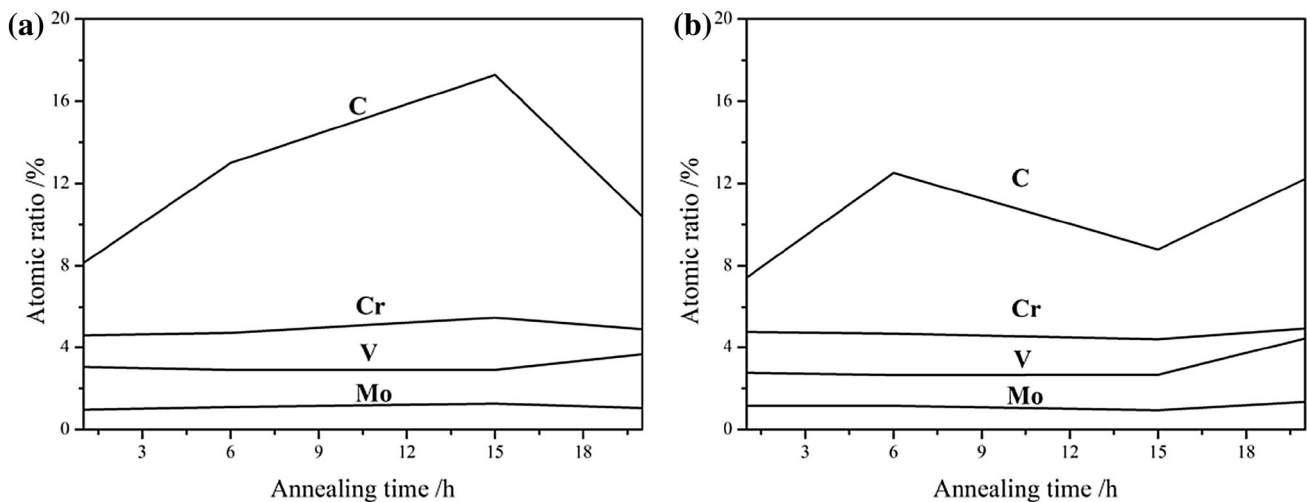
Fig. 10 Variation of element contents in matrix of HSS0 (**a**) and HSS1 (**b**) due to different annealing time

distributed by small size of ferrite and a few weeny carbides after annealing for 15 h. Thus, the hardness is much lower than that of 6 h. The reason for this phenomenon may be that the addition of N promotes the precipitation of nitride or some carbonitride containing alloying elements when the annealing time is long enough. As a result, the precipitation of carbides is restrained. Beyond that, the precipitation phase of carbonitride may also prevent the growth of ferrite grain and play a role in the refinement of ferrite grain size. As the annealing time reaches 20 h in Fig. 9g, h, the matrix of two samples is distributed by a number of clusters which maybe consist of carbides and ferrite. These round structures generally do not possess high hardness, but the clusters which are dispersedly distributed in HSS1 present low density. Moreover, the contents of carbon and other alloying elements in the matrix of HSS1 are slightly higher than those of HSS0 in Fig. 10. It indicates that there are slightly more carbides precipitated in the matrix of HSS1. As a result, the dispersed distributions with more carbides make the hardness of HSS1 higher than HSS0 when the annealing time is 20 h.

4 Conclusions

1. The addition of N and Zr will refine the eutectic structures and enhance the stability of carbides, which are mainly MC, M_2C and M_7C_3. Moreover, a kind of Zr–Si compound which only exists in VC is discovered in HSS1 and this new phase is speculated to be related with the spheroidization of VC.

2. The hardness of two samples is both in a downward trend with the increase of annealing time at 750 °C. However, with the extension of time, the addition of N and Zr makes the decrease of hardness more obvious

by restraining the precipitation of secondary carbides, and the clusters that precipitated from the matrix present lower density but contain more carbides when the annealing time reaches 20 h.

References

[1] Q.X. Liu, D.P. Lu, L. Lu, Q. Hu, Q.F. Fu, Z. Zhou, J. Iron Steel Res. Int. 22 (2015) 245–249.

[2] L. Lu, L.G. Hou, H. Cui, J.F. Huang, Y.A. Zhang, J.S. Zhang, J. Iron Steel Res. Int. 23 (2016) 501–508.

[3] M. Boccalini, H. Goldenstein, Int. Mater. Rev. 46 (2001) 92–115.

[4] Z. Bin, S. Yu, C. Jun, C.Z. Shan J. Iron Steel Res. Int. 18 (2011) 41–48.

[5] X.F. Zhou, D. Liu, W.L. Zhu, F. Fang, Y.Y. Tu, J.Q. Jiang, J. Iron Steel Res. Int. 24 (2017) 43–49.

[6] X.F. Zhou, F. Fang, J.Q. Jiang, J. Mater. Sci. 46 (2011) 1196–1202.

[7] X.F. Zhou, F. Fang, G. Li, J.Q. Jiang, ISIJ Int. 50 (2010) 1151–1157.

[8] L. Lu, L.G. Hou, J.X. Zhang, H.B. Wang, H. Cui, J.F. Huang, Y.A. Zhang, J.S. Zhang, Mater. Charact. 117 (2016) 1–8.

[9] X.H. Zhi, J.D. Xing, H.G. Fu, B. Xiao, Mater. Lett. 62 (2008) 857–860.

[10] X.H. Zhi, J.D. Xing, H.G. Fu, Y.M. Gao, Mater. Charact. 59 (2008) 1221–1226.

[11] S. Kheirandish, S. Mirdamadi, Y.H.K. Kharrazi, Mater. Sci. Technol. 14 (1998) 312–316.

[12] O.A. Bannykh, V.M. Blinov, M.V. Kostina, Met. Sci. Heat Treat. 45 (2003) 43–48.

[13] V.G. Gavriljuk, H. Berns, C. Escher, N.I. Glavatskaya, A. Sozinov, Y.N. Petrov, Mater. Sci. Eng. A 271 (1999) 14–21.

[14] M.J. Wang, Y. Wang, F.F. Sun, Mater. Sci. Eng. A 438 (2006) 1139–1142.

[15] H.J. Xu, Z. Lu, D.M. Wang, C.M. Liu, Fusion Eng. Des. 114 (2017) 33–39.

[16] F.S. Pan, W.Q. Wang, A.T. Tang, L.Z. Wu, T.T. Liu, R.J. Cheng, Nat. Sci. Mater. Int. 21 (2011) 180–186.

[17] H.G. Fu, Foundry 58 (2009) 690–697.

[18] M.J. Wang, L. Chen, Z.X. Wang, E. Bao, J. Rare Earths 30 (2012) 84–89.

[19] B. Jeya Ganesh, S. Raju, A. Kumar Rai, E. Mohandas, M. Vijayalakshmi, K.B.S. Rao, B. Raj, Mater. Sci. Technol. 27 (2011) 500–512.

[20] S. Raju, B. Jeya Ganesh, A. Banerjee, E. Mohandas, Mater. Sci. Eng. A 465 (2007) 29–37.

[21] M.J. Wang, L. Chen, Z.X. Wang, E. Bao, J. Rare Earths 30 (2012) 84–89.

[22] E.T. Turkdogan, Iron Steelmaker 16 (1989) 61–63.

[23] M.J. Wang, Y. Wang, Y.C. Xing, L. Chen, Mater. Sci. Eng. A 438 (2006) 1143–1145.

[24] J.T. Yu, H.Y. Lui, W.H. Zhao, Heavy Cast. Forg. 4 (2012) 14–17.

[25] H.X. Cui, D.S. Ma, H.X. Xu, W.L. Zhu, J.Q. Jiang, J. Iron Steel Res. Int. 23 (2016) 484–488.